

Design of a Flat-Field XUV Spectrometer for Detection of Intense Field High Harmonics

Dhirendra Pratap Singh

*A dissertation submitted for the partial fulfilment
of BS-MS dual degree in Science*



Indian Institute of Science Education and Research Mohali
April 2014

Certificate of Examination

This is to certify that the dissertation titled **Design of a Flat-Field XUV Spectrometer for Detection of Intense Field High Harmonics** submitted by **Dhirendra Pratap Singh** (Reg. No. MS09050) for the partial fulfilment of BS-MS dual degree programme of the Institute, has been examined by the thesis committee duly appointed by the Institute. The committee finds the work done by the candidate satisfactory and recommends that the report be accepted.

Dr. Abhishek Chaudhuri

Dr. Ramandeep S. Johal

Dr. Kamal P. Singh
(Supervisor)

Dated: April 25, 2014

Declaration

The work presented in this dissertation has been carried out by me under the guidance of Dr. Kamal P. Singh at the Indian Institute of Science Education and Research Mohali.

This work has not been submitted in part or in full for a degree, a diploma, or a fellowship to any other university or institute. Whenever contributions of others are involved, every effort is made to indicate this clearly, with due acknowledgement of collaborative research and discussions. This thesis is a bonafide record of original work done by me and all sources listed within have been detailed in the bibliography.

Dhirendra Pratap Singh
(Candidate)

Dated: April 25, 2014

In my capacity as the supervisor of the candidates project work, I certify that the above statements by the candidate are true to the best of my knowledge.

Dr. Kamal P. Singh
(Supervisor)

Acknowledgment

I would like to gratefully acknowledge the support and guidance of my supervisor, Dr. Kamal P . Singh. I would also like to thank Dr. Abhishek Chaudhuri and Dr. Ramandeep S. Johal for assessing my work and discussions. I would also like to thank Dr. Pramod Kumar, Danish Shamoon, Bhupesh Garg, and Gopal Verma for their help and support through out the year.

On a personal note, I would like to thank my family for their support, both financial and moral, which has been without limits throughout my life. Finally, I would like to thank my friends Debi, Soniya, Deepak, Katu, Shivpal, and Mishra for their persistent encouragement and support.

List of Figures

1.1	Harmonic spectrum of Xe gas jet. All odd harmonic between 9 and 21 are visible. The second diffracted order of 21st, 19th and 17th harmonics are also visible at the peaks 101, 112 and 125 respectively. ¹	2
1.2	The relative intensity of the harmonics generated in Xe. ¹	3
1.3	The relative intensity of the harmonics generated in a) Kr and b) Ar. ¹	3
1.4	The three-step model of harmonic generation. ²	5
1.5	Microscopic physics of High order Harmonics generation. ³	5
1.6	(a) The classical electron trajectories (black lines)for different initial phases relative to the IR laser field (gray line). (b) The energy gained by the electron in the continuum as a function of the time when the electron returns to the core. ²	7
2.1	A reflection grating: the incident and diffracted rays lie on the same side of the grating.	10
2.2	The angles of incidence α and diffraction β are shown in relation to the facet angle θ_B for the blaze condition. GN is the grating normal and FN is the facet normal.	12
2.3	Schematic of curved VLS grating. ⁴	13
3.1	Schematic of the Mirror Grating design.	17
3.2	Beam profile of the red laser used for characterization.	18
3.3	Optical setup for Characterisation.	19
3.4	X-Y Profile of the spot size.	19
3.5	Fitted X Profile of the spot size.	20
3.6	Fitted Y Profile of the spot size.	20
3.7	Fitted Tangential focus profile of the spot size.	21
3.8	Plot between incident angle and blaze wavelength.	22
3.9	Plot between different wavelength and diffraction angle for a give incident angle.	23
3.10	Plot of five different order between diffraction angle and wavelength.	23

3.11	Diffraction angle vs. incident angle is plotted for a particular wave length of interest.	24
3.12	Schematic of the VLS grating design.	26
3.13	Optical set up for the flat field spectrometer.	26
3.14	Irradiance plot.	27
3.15	X profile of the irradiance plot.	27
3.16	Focal plane curve for object distance 237 mm.	28
3.17	Focal plane curve for object distance 350 mm.	28
3.18	Proposed 3-D design of the spectrometer.	29
B.1	Creating a new subassembly.	37
B.2	Creating a new lens.	38
B.3	Creating a new simplified source.	38
B.4	Creating a new analysis surface.	39
B.5	Optical setup is complete now any analysis could be performed.	39

List of Abbreviations

HHG	High Harmonics Generation
XUV	Extreme Ultraviolet
VUV	Vacuum Ultraviolet
VLS	Varied Line Space
DPSS	Diode pumped solid state

Abstract

In this project we proposed two design for XUV flat-field spectrometer. Design I consist of a curved mirror and plane grating. As the efficiency of the high harmonics generation process is poor, so we proposed design II in which we used a curved varied line space grating. In case of curved grating the analysis of spectral image and its focusing property is slightly difficult because the image is focused on a curved surface and the detector we are using is flat detector. So we decided to use a curved varied line space grating which focuses on a flat surface. This thesis starts with a introduction to high harmonics generation and the process is explained classically using three step model, scaling laws, trajectories, measurement techniques are discussed in Chapter 1. In Chapter 2, emphasis is on the detection techniques, gratings are main part of the spectrometer so difference between a plane grating, curved grating, and curved VLS grating are discussed. In Chapter 3, the two designs are studied in detail, Matlab simulation and characterisation is done for the design I, FRED and Matlab simulation are done for design II, image focal plane curves are studied and a 3-D design is proposed. All the ground work is done and VLS design is complete and thesis ends with the comparison between the two design in chapter 4.

Contents

List of Figures	i
List of Abbreviations	ii
Abstract	iii
1 Introduction and Theory	1
1.1 High Harmonic Generation	1
1.1.1 Typical Experimental Signature	2
1.2 Theory	4
1.2.1 Three Step Model	4
1.2.2 Trajectories and Semi-classical Picture	6
1.3 Measurement Techniques	7
1.4 Applications	8
2 Detection Techniques	9
2.1 Grating	9
2.1.1 Plane grating	10
2.1.2 Curved Varied Line Space Grating	12
2.2 Flat Field Spectrometer	15
3 Design of XUV Spectrometer	17
3.1 Mirror-Grating Design	17
3.1.1 Characterization of spectrometer using a DPSS Laser	18
3.1.2 Simulation results	22
3.2 VLS Grating Design	25
3.2.1 FRED Simulation	26
3.2.2 Focal plane curves	27
3.2.3 Proposed 3-D Design	29
4 Conclusion and Future Directions	31

A Simulation Details	33
A.1 Curved Grating Simulation	33
A.2 Focal plane Curve Simulation	36
B FRED Simulation	37
B.1 Tutorial	37

Chapter 1

Introduction and Theory

The purpose of this thesis is to design a XUV spectrometer for the detection of the Attosecond pulse. When a short laser pulse of high intensity interacts with the matter, the medium polarises nonlinearly if the strength of electric field of the laser is of the order of binding energy of the electron. One of the interesting effect of this is the generation of the higher frequencies, harmonic, of the driving field. The harmonic wavelength are in the XUV range, 121-10 nm, and short light pulses are generated, a few femtosecond or even attosecond in the length, which are of interest for various applications such as research dealing with fast processes, for example chemical reaction. These type of spectrometer are available in the market but the price is very high and it is possible that the tunability of the spectrometer is not suitable to the range we want to explore.

1.1 High Harmonic Generation

High harmonics generation was first discovered in 1977 with the interaction of intense CO_2 pulse with the plasma generated from solid target.¹ A decade later HHG was generated in gas, in 1987 it was observed by McPherson⁵ and his colleagues and in 1988 by M Ferray et. al. Since the first observation, HHG research has progressed while changing its focus. Initially research was focused on understanding the physics of HHG and then it was shifted to generating a coherent source in the XUV region and now a days it is concentrated in Attosecond science. The whole process from tunnelling ionization followed by radiative recombination during a single optical cycle of the fundamental excitation pulse, is on the attosecond time scale. Therefore, HHG is a unique phenomenon that provides us with a method of observing attosecond quantum dynamics in atoms and molecule.

1.1.1 Typical Experimental Signature

In 1988 M Ferray et. al. reported the observation of very high harmonics of Nd:Yag (1064 nm) laser radiation in the rare gases at an intensity of about $10^{13} \text{ W cm}^{-2}$. Harmonics as high as 33rd harmonics (32.2 nm) was observed in the XUV range in argon. The intensity of harmonics decreased beyond the fifth harmonic as the the order is increased, but beyond 350 nm a UV continuum is obtained extending down towards the short wavelength region in Xenon.

For the physical understanding of the process it is necessary to make further measurements. Detection and spectral analysis could de carried out by using the spectrograph or a monochromater. These high harmonic process have very poor efficiency, so it is important to keep the atomic density up to $10^{17} - 10^{18} \text{ atoms/cm}^3$. The fundamental frequency of a Nd:Yag laser at 1064 nm was used to induce harmonic generation in Xenon, Krypton and Argon. Earlier experiments was done using the short wavelength for the HHG and very little is known about harmonic generation from infrared radiation at 1064 nm at a laser intensity of $10^{13} \text{ W cm}^{-2}$. The picosecond Nd:Yag laser with bandwidth 30 ps and repetition rate of 10 Hz is focused at 0.2 mm from the gas jet nozzle. The XUV light generated at the focal point is analysed along the laser axis using a grazing incidence 275 line/mm gold-coated toroidal holographic grating blazed at 100 nm capable of analysing VUV radiation down to 50 nm. Harmonic spectrum of Xe in the range of 50-130 nm is shown in figure 1.1. All the odd harmonics between 9 and 21 are visible and even the second diffracted order are observed.

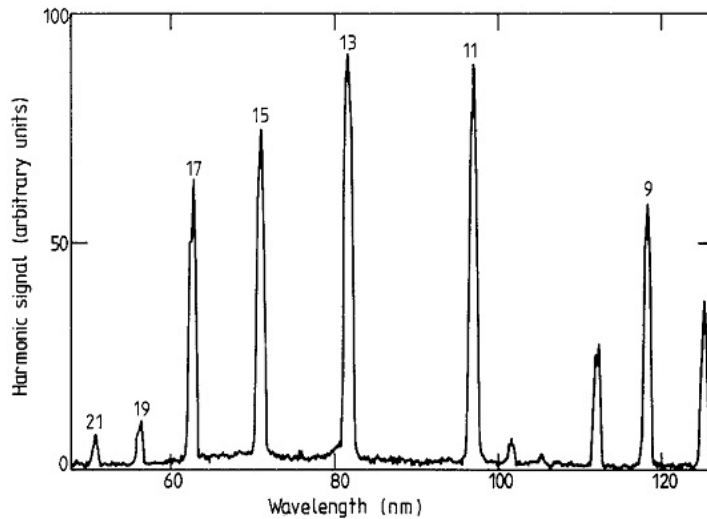


Figure 1.1: Harmonic spectrum of Xe gas jet. All odd harmonic between 9 and 21 are visible. The second diffracted order of 21st, 19th and 17th harmonics are also visible at the peaks 101, 112 and 125 respectively.¹

It is observed by plotting intensities that after fifth order the intensity decreases suddenly and we get a UV continuum. Figure 1.2 shows a plot of the relative intensity for harmonic generation in Xe.

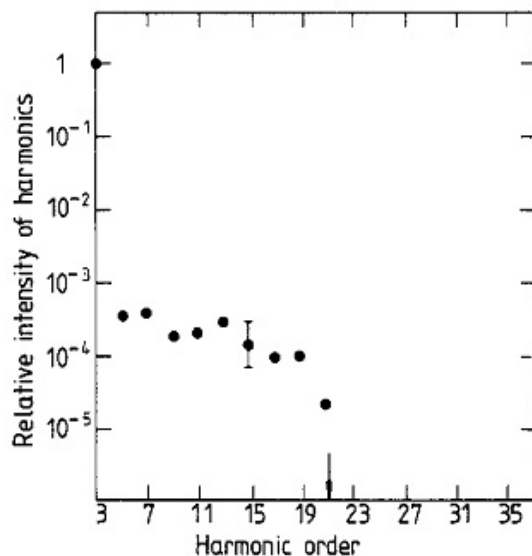


Figure 1.2: The relative intensity of the harmonics generated in Xe.¹

Figure 1.3 and 1.4 are also the intensity plots of Kr and Ar. The harmonic spectrum of Kr and Ar are extended up to 29th order and 33rd order which corresponds to 32.2 nm radiation respectively. The high order generation efficiency of Xe is one order higher than that in Ar.

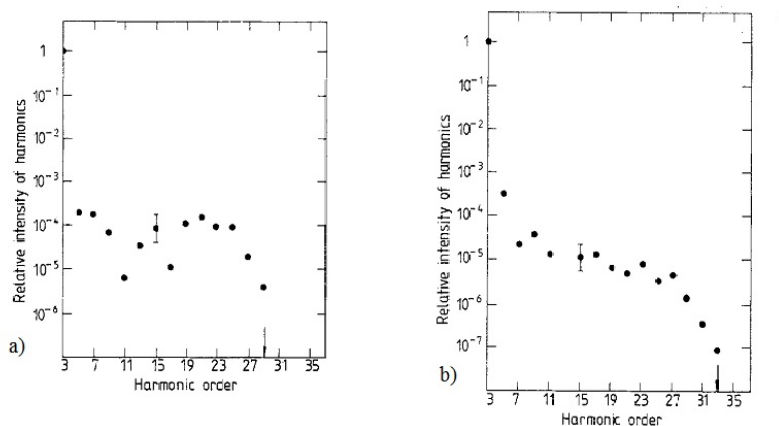


Figure 1.3: The relative intensity of the harmonics generated in a) Kr and b) Ar.¹

In case of Argon, harmonics have also been introduced using a 248 nm laser pulse at an intensity of $10^{15} - 10^{16} \text{ Wcm}^{-2}$ and the shortest wavelength that was observed was 35.5 nm

which is roughly same as 32.2 nm which is induced in Ar by a 1064 nm laser pulse. This means that if we use larger wavelength to generated HHG, then the efficiency of getting short wavelength pulse is higher.

1.2 Theory

The process of high harmonics generation can be understood by semi-classical three step model. To understand quantum mechanically, one has to solve the time dependent Schrödinger equation, which will require huge computational resources. Lewenstein et al. solved this time dependent Schrödinger equation analytically base on some assumption.⁶ 1) single active electron (SAE) approximation, which is that in the process of HHG only one electron of outermost shell is involved 2) adopted two level system which has a ground state and a continuum state, 3) effect of ionization such as ground state depletion is ignored, and 4) in the continuum state the electron wave packet is not affected by Coulomb potential. So it is quite difficult to understand this process quantum mechanically, this semi-classical picture is not fully correct but by calculating the cutoff energy and studying the trajectory plots we can get an idea of the highest order which can be achieved.

1.2.1 Three Step Model

Step 1: Ionization- When induced by a strong (near) infrared laser field, ionization can be approximated by tunnelling; the electron tunnels through the potential barrier created by the ion charge and the laser electric field. Tunnelling determines the ionization probability as a function of time within the wave cycle. For 800-nm light (oscillation period $T_{osc} = 2.7$ fs), tunnelling is most probable during about 300 attoseconds around each field crest near the pulse peak. Thus, the attosecond timescale arises first during tunnelling. Once the electron is split, the attraction of the negative electron to the positive ion rapidly decreases. In contrast, the force that the light exerts on the electron does not depend on how close the electron is to the ion. Therefore, the force exerted by the light wave controls the electron wave packet motion. At first the electric field of the light pushes the wave packet away from the ion, but soon the electric field reverses direction and the force begins to push the electron back. Parts of the wave packet return and pass over their first point of origin.

Step 2: Motion after liberation. A typical electron will gain a kinetic energy of $50 \sim 1,000$ eV from the field during its first femtosecond of freedom, representing tens to hundreds of photons. Therefore, classical mechanics roughly accounts for the electrons motion in the direction of the field. Tunnelling launches electrons on classical trajectories. Each instant of ionization is linked to a moment of recollision by a trajectory. The most important trajectory is populated by electrons born at $T_{osc}/20$ following the peak of the electric field.

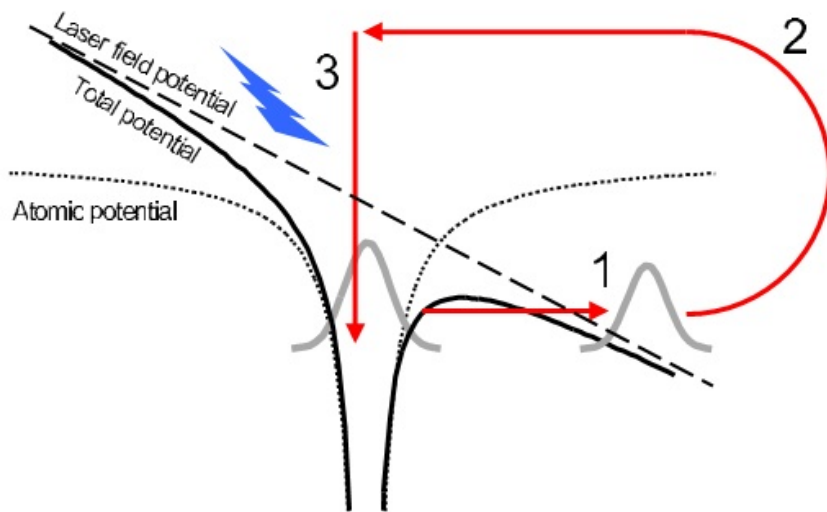


Figure 1.4: The three-step model of harmonic generation.²

These electrons recollide with maximum kinetic energy about $2/3 T_{osc}$ later. The maximum kinetic energy will determine the maximum photon energy in the emitted attosecond photon pulse. It is proportional to the peak electric field E_0^2 and the laser wavelength λ^2 .

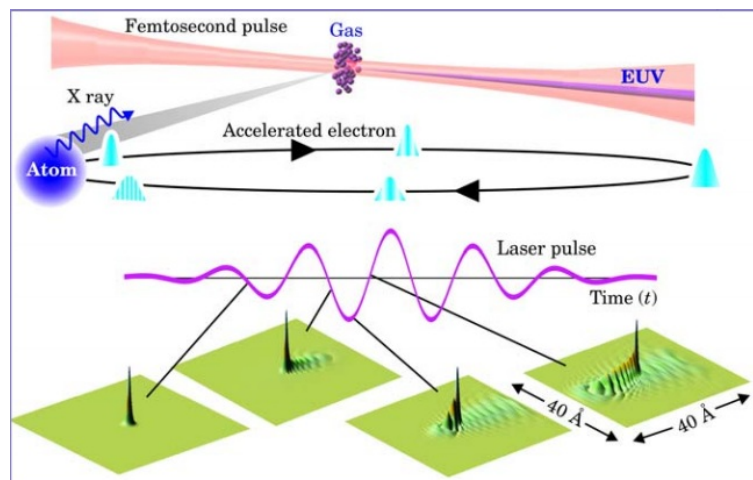


Figure 1.5: Microscopic physics of High order Harmonics generation.³

Step 3: Electronion recollision: Collisions involving energetic particles - particles with kinetic energy 10 eV - occur in much less than one femtosecond. Thus, many phenomena in collision physics are attosecond phenomena. On re-encountering the core, the electron

scatters from its parent ion. Inelastic scattering gives us a chance to validate the semi-classical procedure above, even measuring the equivalent current density. In addition, the recollision electron may give rise to the emission of an attosecond photon burst. In addition to producing attosecond electron and photon pulses, the recollision simultaneously encodes all information on the electron interference. Once the amplitude and phase of the electron interference is encoded in light, powerful optical methods become available to electron interferometry.

The maximum kinetic energy gained after recombining from the acceleration in the fields depends on the time of tunnelling and the time of recombination. The maximum kinetic energy an electron can gain from the laser field is approximately $3.2U_P$,³ where U_P is the ponderomotive energy, which depends upon the fields amplitude and frequency. In the semiclassical picture ponderomotive energy corresponds to average kinetic energy of a free electron in an electric field and is given by

$$U_P = \frac{e^2 E_0^2}{4m\omega^2} \quad (1.1)$$

where e is the electron charge, E_0 is the amplitude of the electric field, ω is the laser angular frequency, and m is the electron mass. The total maximum photon energy that can be achieved through this process is $I_P + 3.2U_P$, where I_P is the ionization potential of the atom. For example, if we use Argon gas for the generation of HHG than we obtained $U_P = 11.9$ eV and Argon has an ionization potential of 15.8 eV, so by calculating the cutoff energy we can easily tell the highest harmonic order that can be observed, in the case of Argon it is 33. This result is verified in the experiment.¹ This process has the twice the frequency as that of laser field used to generate the HHG. The gas is isotropic, so there is no difference if the electron tunnels out when the electric field is $\pm E_0$. So, every time there is phase shift of π , this is the reason why we only get odd harmonics.

1.2.2 Trajectories and Semi-classical Picture

The temporal profile of the emitted dependent on the electron dynamics as the property of emitted pulses are directly to those of the recombining electron. classically studying the trajectories of electron by the electric field of the laser give an intuitive picture of the process. By calculating the electron's maximum energy the corresponding cutoff value can be determined and identify several trajectories contributing to higher order harmonics generation.²

The atom is exposed to a laser field $E(t) = E_0 \sin(\omega t)$. An electron tunnels through the Coulomb barrier and is released into the continuum with zero velocity at time $t = t_i$. The influence of the atomic potential is neglected and assume that the only force experienced by the electron is from the electric field: $F(t) = -eE(t)$, where e is the electron charge. The position of the electron as a function of time $t \geq t_i$ is given by²

$$U_P = \frac{eE_0}{m\omega^2} [\sin(wt) - \sin(wt_i) - w(t - t_i)\cos(wt_i)] \quad (1.2)$$

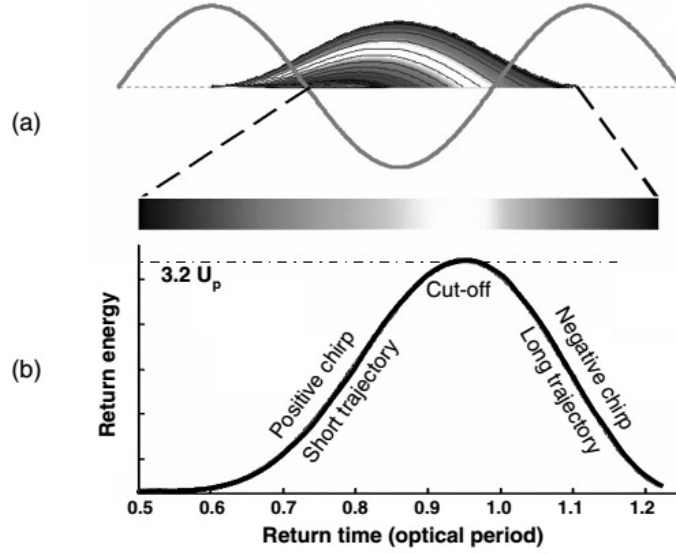


Figure 1.6: (a) The classical electron trajectories (black lines) for different initial phases relative to the IR laser field (gray line). (b) The energy gained by the electron in the continuum as a function of the time when the electron returns to the core.²

In the figure 1.6 we can see that the electron have different trajectories depending on the time when they are tunnelled out and for two different return times we have same return energies. In figure 1.6 (b) in the first half the frequency of the emitted radiation is increasing with the time, so this is called positive chirping, and in the second half the frequency is decreasing with time so it is called chirped.

1.3 Measurement Techniques

Femtosecond optical pulses can be measured by making a replica optical pulse and the two pulses measure each other through a low-order nonlinear optical process in selected materials. The two pulses are combined in a nonlinear crystal phase matched for second harmonic generation. If the two pulses arrive together in the crystal, then the second harmonic is more effectively produced than if the pulses arrive separately in time. The second-harmonic signal measures the overlap of the pulses, and hence their pulse duration. But this process is difficult for attosecond pulses. So instead of measuring the attosecond pulse directly, a photoelectron replica of the attosecond pulse is measured.

Any pulse measurement method must directly or indirectly compare the phase of different Fourier components of a pulse. Autocorrelation, SPIDER and FROG, three extensively used methods to characterize optical pulses, use nonlinear optics to shift the frequency of the Fourier components differentially so that neighbouring frequency components can be compared. The electron-optical streak camera,⁷ an older ultrafast pulse measurement follows a different strategy.⁸ First a photoelectron replica of the optical pulse is produced and then the electron replica is measured. There are two ways to produce the photoelectron replica a) the recollision electron is preexisting replica because its kinetic energy, amplitude and phase are transferred to the attosecond pulse when it recombine the atom, b) the attosecond optical pulse itself can be used to photoionize the atomic media to produce a new electron replica. The latter has been applied to measure isolated attosecond pulses or attosecond trains.

1.4 Applications

Attosecond technology is capable of attosecond time resolution. Attoseconds are the time scale for electron motion. A classical electron completes a Bohr orbit in about 150 as. Although quantum mechanics says that the Bohr orbit is not observable, it does allow us to observe something comparable. So it is one way to measure this bound-state electron wave packet with attosecond precision. So far, attosecond pulses have been used for triggering or for probing dynamics. Their low flux has prevented them from being applied simultaneously as pump and probe. Scaling waveform-controlled few-cycle light to relativistic intensities holds promise for producing high-intensity attosecond photon pulses in the extreme ultraviolet and soft-X-ray regime that can be simultaneously applied for both purposes. The most promising route to this goal is to expose a solid surface to relativistic-intensity light. The light creates a plasma mirror that oscillates with a velocity approaching that of light. This imposes a relativistic Doppler up-shift of the reflected incident light. If the light pulse contains only several cycles then the reflected blue-shifted photons can be delivered in a single, ultra-intense attosecond ultraviolet or soft-X-ray pulse.⁹ These pulses will enable attosecond pump/attosecond probe spectroscopy. Real-time observation and control of charge transfer in molecular systems will become feasible for the first time. Molecular electronics,¹⁰ bioinformatics and cancer research may benefit from these capabilities.

Chapter 2

Detection Techniques

Spectrometer is a general class of instrument that collects, spectrally disperses, and reimages an optical signal. The output signal is series of monochromatic images corresponding to the wavelengths present in the light imaged at the entrance slit. Its principal components are monochromator and a detector such as a photoemissive cell or a photomultiplier tube.

A spectrometer consist of the following elements:

1. An entrance slit or aperture stop.
 2. A collimating element, it can be a lens, a mirror or an integral part of the dispersing element, as in a concave grating spectrometer.
 3. A dispersing element, usually a grating which spreads the light intensity in space as a function of wavelength.
 4. A focusing element to form an image of the entrance slit at some convenient focal plane.
- In this thesis we have discussed two type design, and did simulation for both the design. Design I is mirror-grating design, in which plane grating is used and a toroidal mirror is used to remove the astigmatism. Design II is Curved Varied Line Space grating design, in which only a curved grating is used. In this type of grating, line density across the surface is not constant as in the standard grating but varies with the distance from the center.¹¹

2.1 Grating

Diffraction grating is an optical element with a periodic structure, which splits and diffracts light into several beams travelling in different direction. For practical application, grating generally have ridges on the surface other than dark lines.

Grating can be of the reflective or transmissive type, a grating has a zero order mode ($m = 0$), in which there is no diffraction and a ray of light behaves accordingly to law of reflection and refraction.

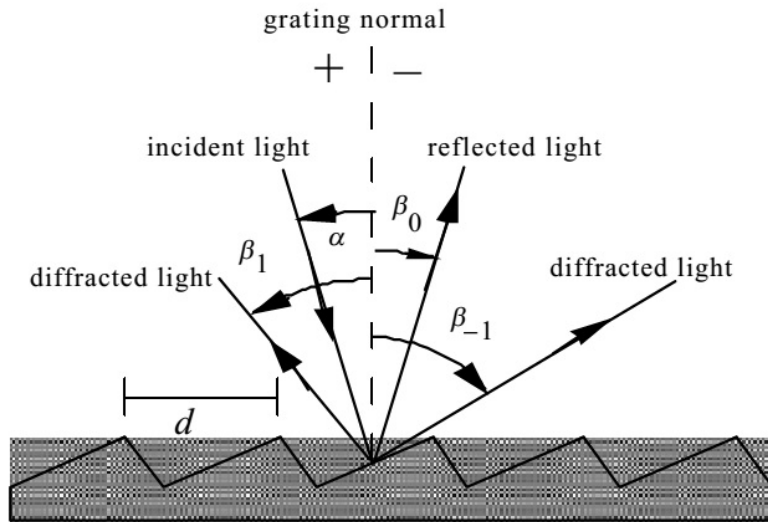


Figure 2.1: A reflection grating: the incident and diffracted rays lie on the same side of the grating.

2.1.1 Plane grating

Plane diffraction gratings are manufactured either classically with the use of a ruling engine by brushing grooves with a diamond stylus or holographically with the use of interference fringes generated at the intersection of two laser beams. The gratings are usually designated by groove density, the number of grooves per mm, also equal to the inverse of the groove period. The groove period must be of the order of the wavelength of interest. The maximum wavelength that a grating can diffract is equal to twice the grating period. When groove spacing is less than half the wavelength of the light, the only present order is $m = 0$. The grating equation can be derived by calculating the path difference:

$$\text{Path difference} = d(\sin\alpha + \sin\beta)$$

For maxima,

$$d(\sin\alpha + \sin\beta) = m\lambda$$

where,

d is groove spacing

α is incident angle

β is diffraction angle

λ is wavelength of interest

Angular Dispersion:

It is a measure of the separation (either angular or spatial) between diffracted light of different wavelength. In a given spectral order m , the different wavelength of polychromatic wavelength incident at angle α are separated in angle. For groove spacing d , the relationship between the λ , α , and β :

$$\beta(\lambda) = \sin^{-1}\left(\frac{m\lambda}{d} - \sin\alpha\right) \quad (2.1)$$

when $m = 0$, the grating acts as a mirror and wavelengths are not separated and this is called specular reflection or zero order.

The change D (Angular Dispersion) in the diffraction angle per unit wavelength is therefore:

$$D = \frac{d\beta}{d\lambda} \quad (2.2)$$

$$= \frac{m}{d\cos\beta} \quad (2.3)$$

$$= \frac{m\sec\beta}{d} \quad (2.4)$$

$$= Nm\sec\beta \quad (2.5)$$

As the groove frequency N increases the angular dispersion increases. Substituting the general equation into the dispersion:

$$D = \frac{d\beta}{d\lambda} = \frac{\sin\alpha + \sin\beta}{\lambda\cos\beta} \quad (2.6)$$

For the given wavelength, D is solely a function of angles. If we consider the Littrow Configuration: $\alpha = \beta$:

$$D = \frac{2\tan\beta}{\lambda} \quad (2.7)$$

Linear Dispersion

For a given diffracted λ i order m (which corresponds to an angle of diffraction β), the linear dispersion of a grating system is the product of the angular dispersion D and the effective focal length $r'(\beta)$ of the system

$$r' D = Nm r' \sec\beta \quad (2.8)$$

Resolving Power

The resolving power of grating is a measure of its ability to separate adjacent spectral line of average wavelength.

$$R = \frac{\lambda}{\Delta\lambda} \quad (2.9)$$

The theoretical resolving power of planar diffraction grating is

$$R = mN \quad (2.10)$$

$$R = \frac{Nd(\sin\alpha + \sin\beta)}{\lambda} \quad (2.11)$$

where m is diffraction order and N is the total number of grooves illuminated.

Blazed Grating

Blazed grating produce maximum efficiency at desired λ into any order, other than $m = 0$. In blazed grating the grooves of the grating are controlled to form right angle triangle with a blaze angle θ_B . Littrow condition: It is the condition when the incident angle and

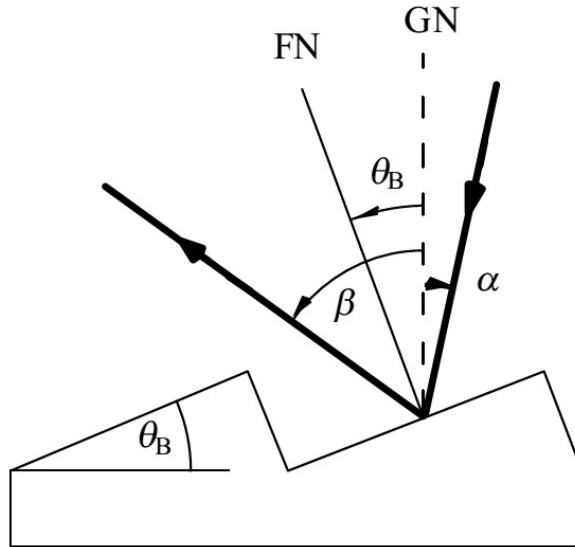


Figure 2.2: The angles of incidence α and diffraction β are shown in relation to the facet angle θ_B for the blaze condition. GN is the grating normal and FN is the facet normal.

diffraction angle are equal to the blaze angle of the grating

$$\alpha = \beta = \theta_B$$

$$\sin\alpha + \sin\beta = \frac{m\lambda}{d}$$

$$2\sin\theta_B = \frac{m\lambda}{d} \quad (2.12)$$

2.1.2 Curved Varied Line Space Grating

A concave reflection grating can be modelled as a concave mirror that disperses. In these types of grating line density across the surface is not constant as in the standard grating

but varies with the distance from the center. Curved grating forms an image at circular plane which called Rowland circle,¹² where as curved VLS grating forms an image at a flat surface.

To analyse its spectral image focusing property an analytical method is used which uses the Fermat's principle which requires calculation of the light path function.¹³ The origin

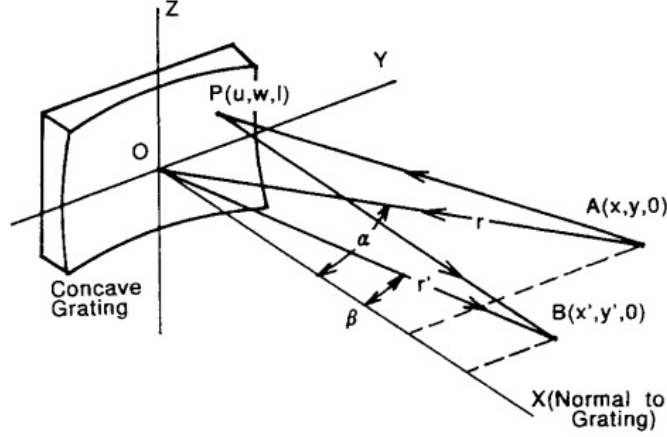


Figure 2.3: Schematic of curved VLS grating.⁴

of the coordinate system O is on the vertex of the concave grating sphere. The x-axis is normal to the concave surface at O, and the y-axis is perpendicular and the z-axis is parallel to the grating groove at O. To optimize the spectral image-focusing of properties of the spectrometer, a light source is placed at a point $A(x, y, 0)$ in the x-y plane and point $B(x', y', 0)$ is a nominal focal point of a spectrum wavelength λ diffracted in the m th order by the grating.⁴

For the ray that is emitted from the point A, diffracted at $P(u, w, l)$ on the grating surface, and passes through nominal focal point B, the light path function is defined as

$$F = \langle AP \rangle + \langle PB \rangle + nm\lambda \quad (2.13)$$

where n is the groove number at P counted from O. According to Fermat's principle, stigmatic spectral image focusing is obtained when the following condition are satisfied simultaneously:

$$\frac{\delta F}{\delta w} = 0, \frac{\delta F}{\delta l} = 0 \quad (2.14)$$

In the Eq. (2.14) the distances AP and PB are expressed by

$$\langle AP \rangle^2 = (x - u)^2 + (y - w)^2 + l^2$$

$$\langle BP \rangle^2 = (x' - u)^2 + (y' - w)^2 + l^2$$

Using the polar coordinate system with $x = r\cos\alpha$, $y = r\sin\alpha$, $x' = r'\cos\beta$, and $y' = r'\sin\beta$, we have

$$\begin{aligned} \langle AP \rangle &= r^2 + u^2 + l^2 - 2ur\cos\alpha - 2wr\sin\alpha \\ \langle BP \rangle &= r'^2 + u^2 + l^2 - 2ur'\cos\alpha - 2wr'\sin\alpha \end{aligned}$$

where α and β are the angles of incidence and diffraction, respectively at O.

The substrate used for the concave grating is a spherical substrate, therefore the coordinates of the point P on the spherical surface with radius of curvature R satisfies the following condition:

$$(u - R)^2 + w^2 + l^2 = R^2 \quad (2.15)$$

By expanding the above equation into power series of w and l we have

$$u = \frac{w^2 + l^2}{2R} + \frac{(w^2 + l^2)^2}{8R^3} + \frac{(w^2 + l^2)^3}{16R^5} + \dots \quad (2.16)$$

The grooves number n on the VLS grating is defined as

$$n = \frac{1}{\sigma_0} \left(w + \frac{b_2}{R}w^2 + \frac{b_3}{R^2}w^3 + \frac{b_4}{R^3}w^4 + \dots \right), \quad (2.17)$$

where σ_0 is the groove spacing at O and b_2, b_3, b_4, \dots are the ruling parameter for the space variation.¹⁴

The light function function, is now expressed in the power of w and l :

$$F = r + r' + wF_{10} + w^2F_{20} + l^2F_{02} + w^3F_{30} + wl^2F_{12} + w^4F_{40} + w^2l^2F_{22} + l^4F_{04} + T(w^5), \quad (2.18)$$

where $T(w^5)$ are terms in w^5 or higher.

In Eq. (2.19) every F_{ij} terms can be expressed as

$$F_{ij} = C_{ij} + \frac{m\lambda}{\sigma_0} M_{ij} \quad (2.19)$$

The explicit expression for C_{ij} and M_{ij} are

$$C_{10} = -\sin\alpha - \sin\beta. \quad (2.20)$$

$$M_{10} = 1, \quad (2.21)$$

$$C_{20} = \frac{1}{2} \left(\frac{\cos^2\alpha}{r} - \frac{\cos\alpha}{R} \right) + \frac{1}{2} \left(\frac{\cos^2\beta}{r'} - \frac{\cos\beta}{R} \right), \quad (2.22)$$

$$M_{20} = \frac{b_2}{R}, \quad (2.23)$$

$$C_{02} = \frac{1}{2} \left(\frac{1}{r} - \frac{\cos\alpha}{R} \right) + \frac{1}{2} \left(\frac{1}{r'} - \frac{\cos\beta}{R} \right), \quad (2.24)$$

$$M_{02} = 0, \quad (2.25)$$

The benefits of the VLS grating appears in the tangential focus where the focal length becomes subject to modification by the first order line density coefficient, b_2 .¹⁵

$$F_{20} = \left(\frac{\cos^2 \alpha}{r} - \frac{\cos \alpha}{R} \right) + \left(\frac{\cos^2 \beta}{r'} - \frac{\cos \beta}{R} \right) + \frac{2N_0 m \lambda b_2}{R} \quad (2.26)$$

The Tangential focal point:

$$r' = \frac{r R \cos^2 \beta}{r(\cos \alpha + \cos \beta - \frac{2m\lambda b_2}{N_0}) - R \cos^2 \alpha} \quad (2.27)$$

First order line density coefficient, b_2 .

$$b_2 = \frac{\cos \alpha + \cos \beta - \left(\frac{R \cos^2 \alpha}{r} + \frac{R \cos^2 \beta}{r'} \right)}{2(\sin \alpha + \sin \beta)} \quad (2.28)$$

2.2 Flat Field Spectrometer

For the detection intense field high harmonics using a flat field spectrometer we have proposed two designs. Spectrometer is an instrument designed to measure the distribution of radiation in a particular wavelength region. In design I optics consists of a concave mirror and a plane grating, in most of the cases a toroidal mirror is used to reduce the astigmatism and the grating separates the different wavelength in different diffraction angles.

Design II optics consists of a curved varied line space grating. If we use only concave grating than to analysis it's image and focusing property, we have to use a Rowland mount spectrometer. So to get an focus on a surface which is almost flat we use curved varied line space grating. In these types of grating the tangential focus is subjected to the modification of the first order grating parameter. In the next chapter both of these designs are studied in details, simulation and characterisation are done for the two designs.

Chapter 3

Design of XUV Spectrometer

In this project I worked on the design of two types of spectrometer. Design I consists of a toroidal mirror to focus the incoming radiation at the detector and the optical element is plane diffraction grating. Here toroidal mirror is used to correct the astigmatism at the detectors surface. Design II consists of a curved varied space line grating with a normal groove density of 1200 grooves/mm. The speciality of this grating is that its groove density varies across the grating with equation:

$$N(w) = N_0 \left(1 + \frac{2b_2w}{R} + \frac{3b_3w^3}{R^2} + \dots \right) \quad (3.1)$$

3.1 Mirror-Grating Design

Below is the schematic of the Mirror-Grating, after the generation of HHG the radiations are focused to a point source using a lens and then it is further focused using a mirror to get an image at XUV detector. In this case usually a toroidal mirror is used to get rid of the astigmatism at point of image formation.

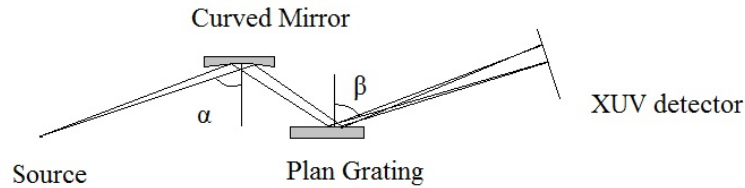


Figure 3.1: Schematic of the Mirror Grating design.

3.1.1 Characterization of spectrometer using a DPSS Laser

The red laser, $\lambda = 630 \text{ nm}$ is used to characterize the Design I. First beam profile was measured using the beam profiler.

Beam Profile:

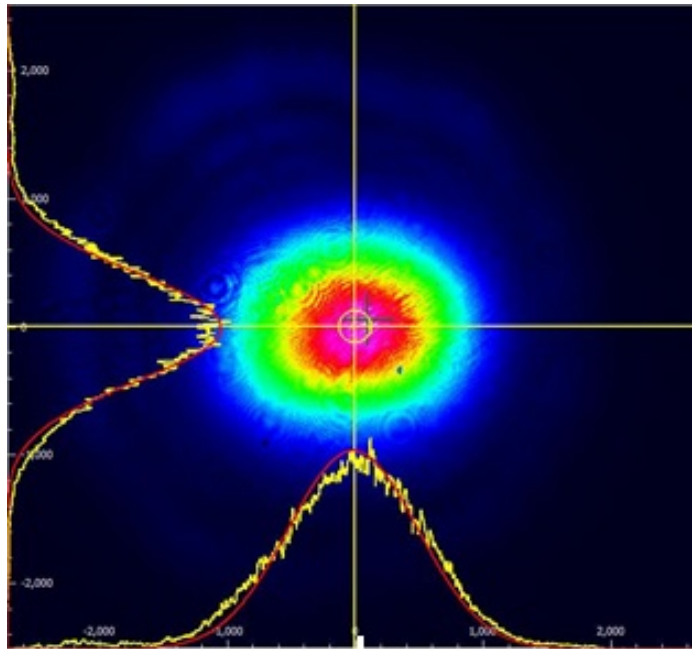


Figure 3.2: Beam profile of the red laser used for characterization.

Beam width:

$$X = 2.2 \text{ mm}$$

$$Y = 1.8 \text{ mm}$$

Optical setup is designed for the Mirror-grating design

$$\text{Incident angle, } \alpha = 65.25^\circ$$

For Order, $m = 1$

$$\text{Diffraction angle, } \beta = 31.95^\circ$$

Distance of focus of lens form grating: $u = 50 \text{ cm}$

Distance between grating and mirror: $d = 6 \text{ cm}$

Beam was focused using the lens of focal length, $f = 30 \text{ cm}$, measured focal length is, $f = 29.8 \text{ cm}$. The X-Y profile of this focused spot before the grating was measured and

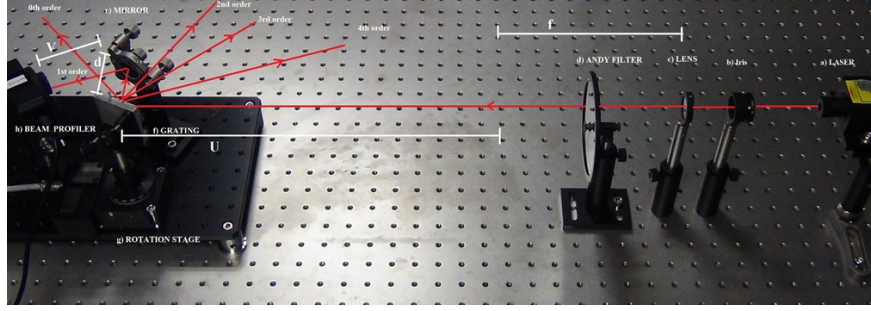


Figure 3.3: Optical setup for Characterisation.

curve fitting was done using the equation:

$$W(z) = w_0 \sqrt{1 + \left(\frac{z}{z_r}\right)^2} \quad (3.2)$$

Measured X-Y in figure 3.4 profile of the spot size within the Rayleigh Range:

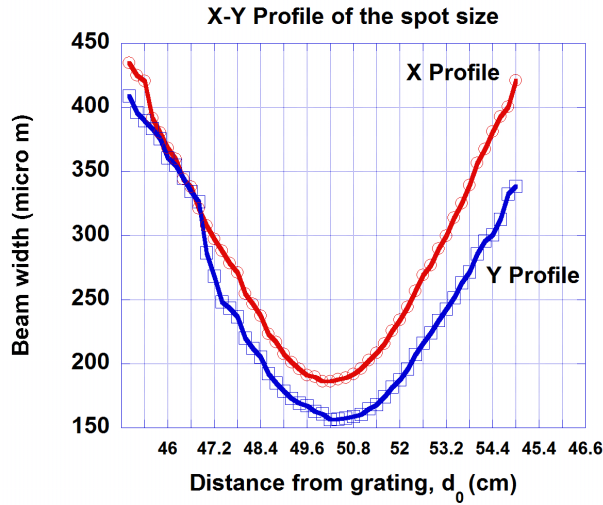


Figure 3.4: X-Y Profile of the spot size.

Individual X and Y in figure 3.5 and 3.6 curves are fitted and spot size and Rayleigh range is calculated:

X profile:

Object Distance, $u = 56$ cm

Beam waist, $w_0 = (188.30 \pm 2.3)\mu\text{m}$

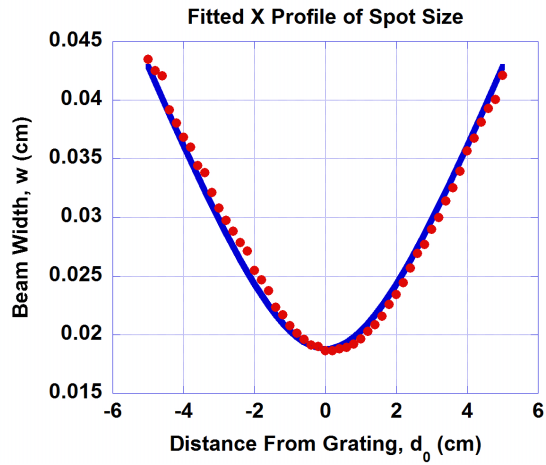


Figure 3.5: Fitted X Profile of the spot size.

$$\text{Rayleigh range, } z_r = (2.44 \pm 0.05) \text{ cm}$$

Y Profile:

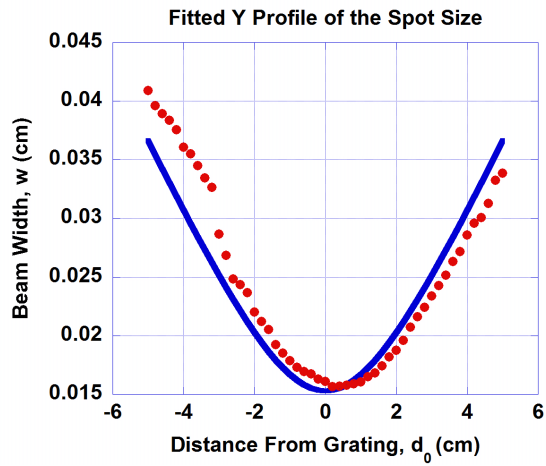


Figure 3.6: Fitted Y Profile of the spot size.

$$\text{Object Distance, } u = 56 \text{ cm}$$

$$\text{Beam waist, } w_0 = (153.05 \pm 4.73) \mu\text{m}$$

$$\text{Rayleigh range, } z_r = (2.16 \pm 0.10) \text{ cm}$$

Finally beam profile of the final focus is measured, the focal length of the mirror is, $f = 10$ cm and curve fitting was using the same equation,

Tangential Focus:

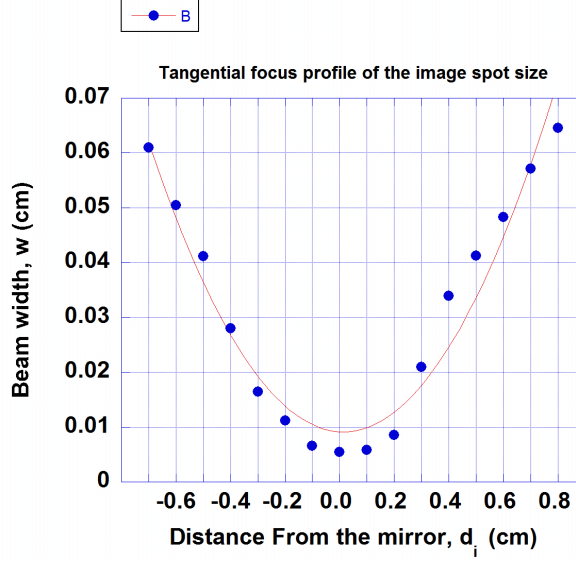


Figure 3.7: Fitted Tangential focus profile of the spot size.

Image Distance, $u = 8.7$ cm

Beam waist, $w_0 = (21.04 \pm 0.0037)\mu m$

Rayleigh range, $z_r = (0.026 \pm 0.047)$ cm

Finally magnification of beam waist was measured by two ways: spot size and object-image distance:

Spot size:

$$m = \frac{w'_0}{w_0} = \frac{21.04}{188.30} = 0.112$$

where w'_0 is spot size of the tangential focus of the image and w_0 is spot size of the object (X profile).

Object image distance:

$$m = -\frac{v}{u} = \frac{8.7}{56} = 0.155$$

where v is the image distance of tangential focus and u is the object distance.

The error in result is because the image distance measurement of the final focus was varying within mm so its not measured accurately, it is only main source of error.

3.1.2 Simulation results

Mirror-Grating Design is also simulated in Matlab. The wavelength which is scanned is from 30 ~ 80 nm. In this range the blaze wavelength considered is, $\lambda_B = 50\text{nm}$. Blaze angle of the grating is considered to be, $\theta_B = 3.2^\circ$.

Littrow wavelength:

$$\lambda_L = \frac{2\sin\theta_B}{N} \quad (3.3)$$

Relation between blaze wavelength and incident angle:

$$\lambda_B = \lambda_L \cos(\alpha - \theta_B) \quad (3.4)$$

Calculated incident angle:

$$\alpha = \cos^{-1}\left(\frac{\lambda_B}{\lambda_L}\right) + \theta_B \quad (3.5)$$

$$\alpha = 60.68^\circ$$

The two diffraction angles are calculated using grating equation

$$\beta_1 = -53.3^\circ$$

$$\beta_2 = -50.8^\circ$$

Different plots were analysed using Matlab. For this simulation the blaze wavelength, $\lambda_B =$

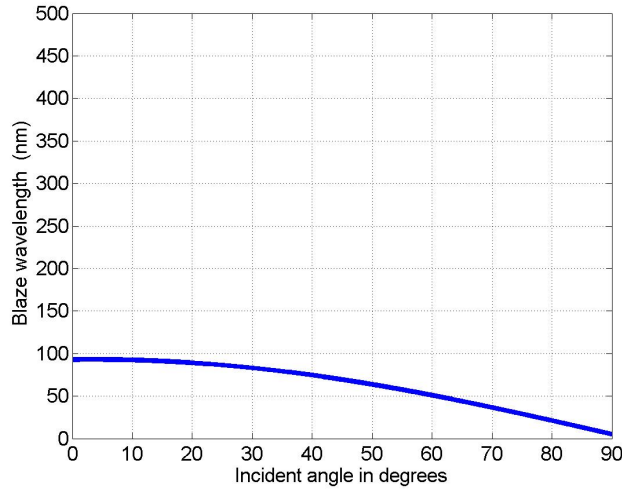


Figure 3.8: Plot between incident angle and blaze wavelength.

50 nm. From the graph figure 3.8, it can be seen that the to work for blaze wavelength lower than 50 nm, the incident angle should be increased accordingly. In this simulation the incident angle is, $\alpha = 60.68^\circ$. For this range of wavelength the difference in the diffraction angle of the two wavelength is less than 4° .

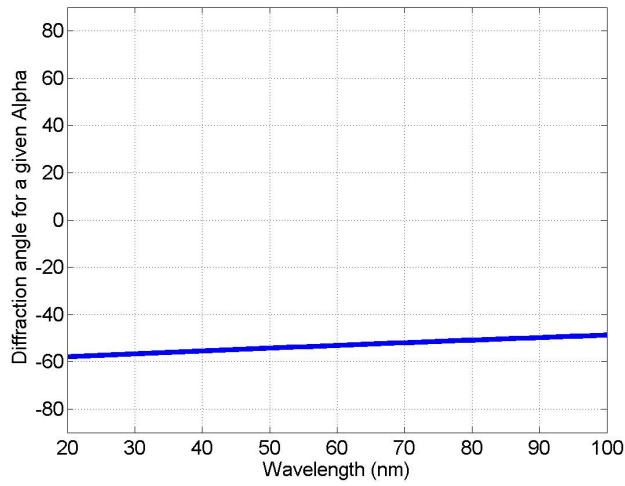


Figure 3.9: Plot between different wavelength and diffraction angle for a give incident angle.

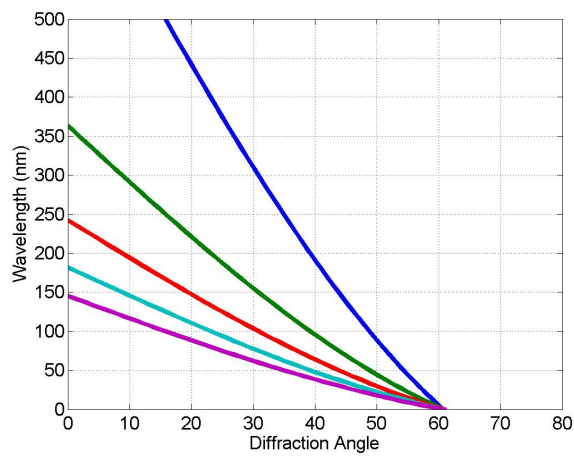


Figure 3.10: Plot of five different order between diffraction angle and wavelength.

At this angle of incident the different order are overlapping in this wavelength range figure 3.10. By increasing the incident it might be possible to over come this problem.

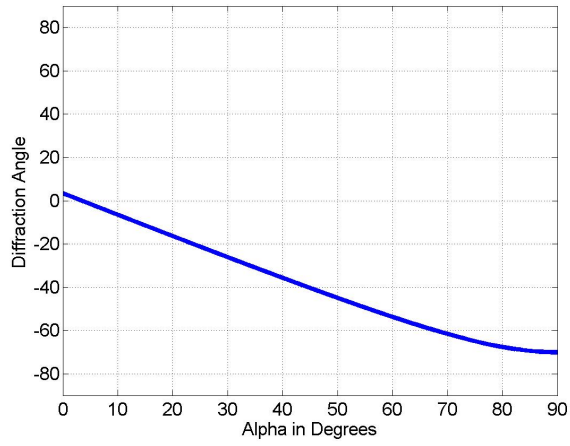


Figure 3.11: Diffraction angle vs. incident angle is plotted for a particular wave length of interest.

In figure 3.11 the wavelength of interest is 50 nm, as we increase the incident angle the diffraction angle is saturating around 70° .

3.2 VLS Grating Design

Curved Varied Line Space design is the main design. In this design we are using only curved varied line space grating. Simple curved grating focus only on the curved surface, so we either use a Rowland Circle spectrometer or can use a VLS grating which focuses on a flat surface. In these type of grating line density across the surface is not constant, as in the standard grating but varies with the distance from the center.

The variation is described by the polynomial:

$$N(w) = N_0 \left(1 + \frac{2b_2 w}{R} + \frac{3b_3 w^3}{R^2} + \dots \right) \quad (3.6)$$

where N_0 is the line density at the origin and coefficients b_i are the design parameters.

The effect of VLS grating can be determined by replacing N by $N(w)$ and again redefining the coefficients in the path difference equation.

Tangential focus:

$$F_{20} = \left(\frac{\cos^2 \alpha}{r} - \frac{\cos \alpha}{R} \right) + \left(\frac{\cos^2 \beta}{r'} - \frac{\cos \beta}{R} \right) + \frac{2N_0 m \lambda b_2}{R} \quad (3.7)$$

The benefits of the VLS grating appears in the tangential focus where the focal length becomes subject to the modification by the first order line density coefficient, b_2 .

The Tangential focal point:

$$r' = \frac{r R \cos^2 \beta}{r (\cos \alpha + \cos \beta - \frac{2m\lambda b_2}{N_0}) - R \cos^2 \alpha} \quad (3.8)$$

First order line density coefficient, b_2 .

$$b_2 = \frac{\cos \alpha + \cos \beta - \left(\frac{R \cos^2 \alpha}{r} + \frac{R \cos^2 \beta}{r'} \right)}{2(\sin \alpha + \sin \beta)} \quad (3.9)$$

The grating that is ordered is for the range 5 ~ 20 nm. So to fit it in our range first we have to calculate the first order line density coefficient.

For 5 nm the first order line density coefficient,

$$b_2 = -20.119$$

For 20 nm the first order line density coefficient,

$$b_2 = -20.057$$

Calculated mean value of $b_2 = -20.12$, using the given parameters of grating.

Schematic:

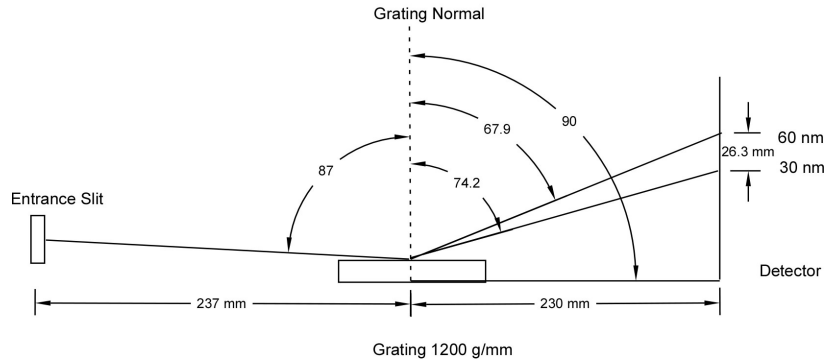


Figure 3.12: Schematic of the VLS grating design.

3.2.1 FRED Simulation

To get a better understanding of how XUV flat-field spectrometer works and examine its properties a ray tracing program, FRED from Photon Engineering, is used. The optical setup is constructed according to the schematic.

The source of the HHG is modelled as a point source with an angular spread of 1 mrad (0.0573°). The grating is designed with the groove density 1200 grooves/mm. An analysis plane is placed perpendicular to the grating at the focus point.

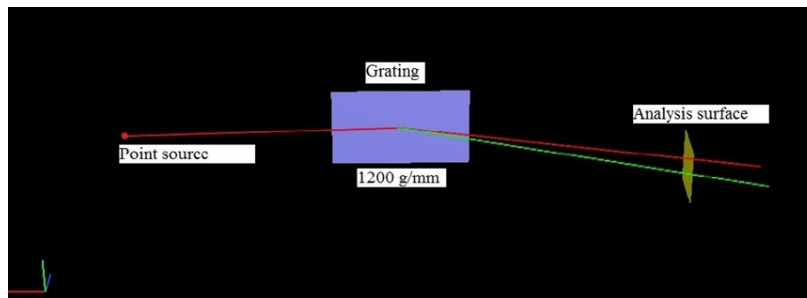


Figure 3.13: Optical set up for the flat field spectrometer.

Irradiance spread function is plotted for this set up in figure 3.14. The two different wavelength were selected 30 nm and 60 nm. Decrease in the intensity can be clearly observed as a function of the wavelength.

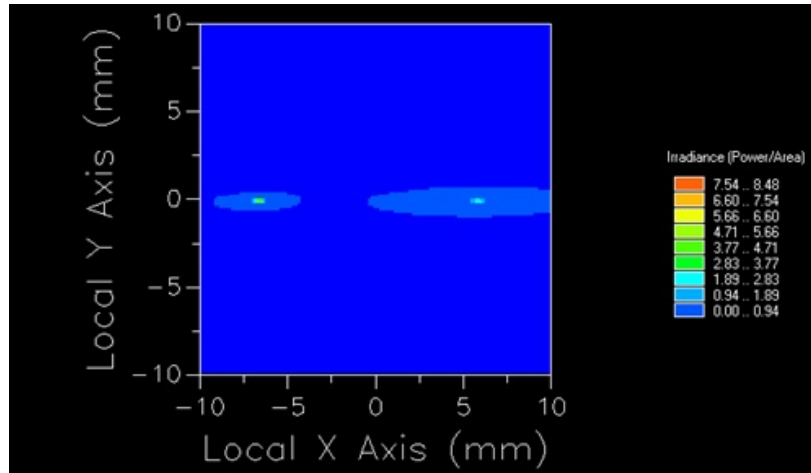


Figure 3.14: Irradiance plot.

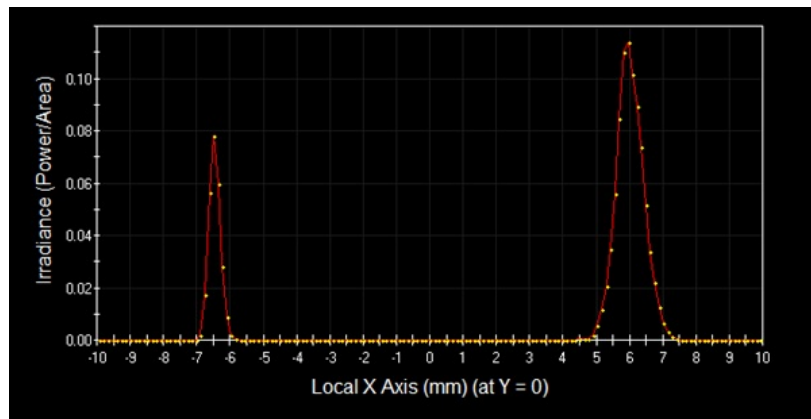


Figure 3.15: X profile of the irradiance plot.

3.2.2 Focal plane curves

The grating manufacturer's designed incidence angle α , object distance r , and image distance r' of the XUV grating are 87° , 237 mm, and 235 mm respectively. The spectrum range it covered is from 5 ~ 20 nm. Since the grating in our setup is not being used with its manufacturer's design parameters, so the focal plane curves¹⁶ of different incidence angle and for two different object distance with a spectrum range from 30 to 60 nm are plotted using Matlab.

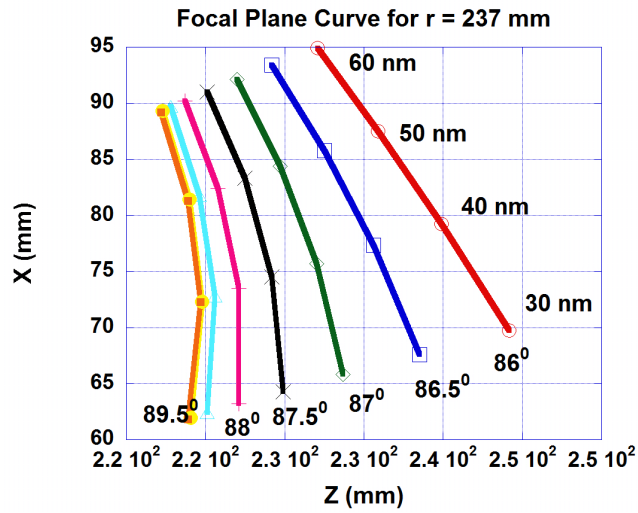


Figure 3.16: Focal plane curve for object distance 237 mm.

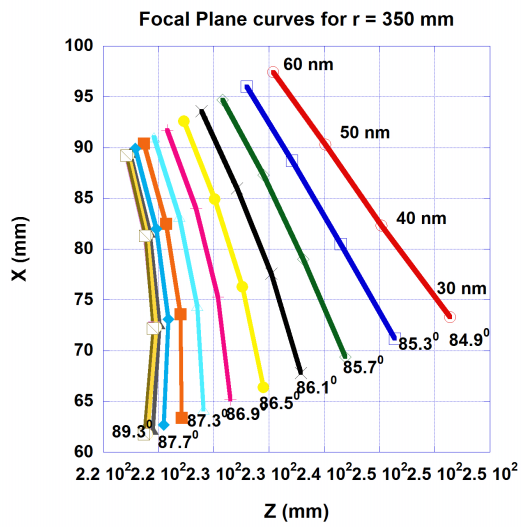


Figure 3.17: Focal plane curve for object distance 350 mm.

3.2.3 Proposed 3-D Design

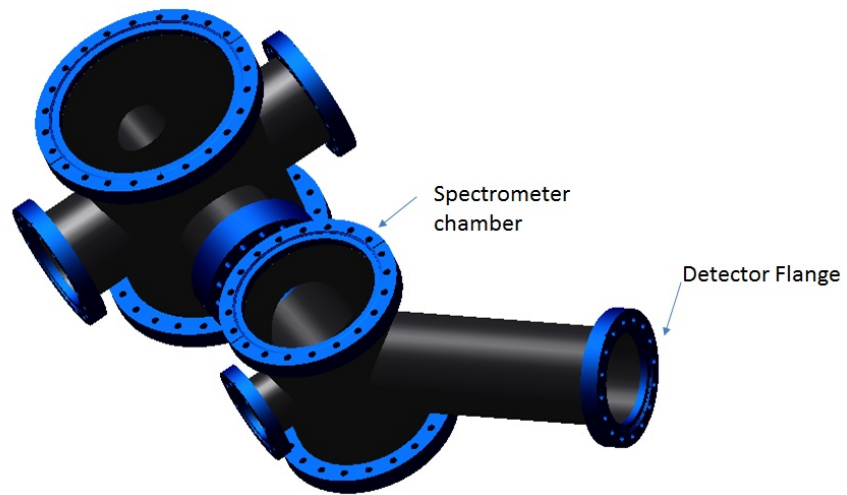


Figure 3.18: Proposed 3-D design of the spectrometer.

Chapter 4

Conclusion and Future Directions

Studying the theory of the grating, I learned the image focusing properties of the curved and curved VLS grating and the benefits of the VLS grating over curved grating. Matlab simulations further helped in understanding the focusing property of VLS grating. Further we did FRED simulation of VLS design and image focal plane curves are studied for two different object distances. Both mirror-grating design and VLS design are analysed and studied in detail.

There are few drawbacks of the mirror-grating design. First, the degree of freedoms in this type of spectrometer are more than the VLS spectrometer and it is more difficult to stabilise the spectrometer. Second, the efficiency of the high harmonics generation process is poor, and every time it reflects from an optical element some part of it gets absorbed, so this further reduces the efficiency of the process.

By using curved VLS grating we have reduced the degree of freedom and it is more easy to align and handle the optics. By reducing one optical element we have increased the efficiency of the process by preventing external loss. In the VLS grating design we can also get the focus on a flat surface because in these types of grating, line density across the surface is not constant as in the standard grating but varies with the distance from the center and the benefit of the VLS grating appears in the tangential focus where the focal length becomes subject to the modification by the first order line density coefficient. So, we are choosing VLS grating design over mirror-grating design for the further detection of intense field high harmonics.

For the future directions, FRED software used in this thesis is a Demo version, so some simulation were not possible because of the limitation of the software. These simulation could be performed again with the full version of the software. Almost all the parts and essential components have been ordered, as soon as the design of vacuum chamber is complete, we will assemble the whole setup and finally we will probe the higher harmonics.

Appendix A

Simulation Details

These are details of the Matlab programs used for simulating curved grating and plotting the focal plane curves.

A.1 Curved Grating Simulation

```
close all
alpha = 0:0.1:90;
lambda = 0:1:500;
beta = 0:1:80;
betaRad = beta*pi/180;
alphaRad = alpha*pi/180; % angle of incidence
phi = 3.2*pi/180; % blaze angle
gr_den = 1200; % groove density per mm
d = 1E-3/gr_den; % groove spacing in meters
spot = 1; % normal spot size in mm
order = 1;
inc_lambda = 50E-9; % wavelength of interest
lambda_Litt = 2*sin(phi)*d; % Littrove wavelength
display(lambda_Litt*1E9);
alpha_1 = acos(inc_lambda/lambda_Litt) + phi;
display(alpha_1*180/pi);

% now we find the blaze wavelength as a function of incident angle alpha

lambda_blaze = (lambda_Litt*cos(alphaRad - phi)*1E9)/order;
diff_angle = asin((order*inc_lambda/d) - sin(alphaRad))*180/pi; % diff. angle vs incident
angle
```

```
diff_angle_1 = asin((order*lambda*1E-9/d) - sin(alpha_1))*180/pi; % diff. angle vs wave-  
length
```

```
lambda_1 = 833.33*(sin(alpha_1) - sin(betaRad));
```

```
    % plot  
plot(alpha, lambda_blaze)  
axis([0 90 0 500]);  
grid on  
xlabel('alpha in degrees')  
ylabel('Blaze wavelength in nm')
```

```
    figure  
plot(alpha, diff_angle)  
axis([0 90 -90 90]);  
grid on  
xlabel ('alpha in degrees')  
ylabel ('Diffraction angle for wavelength of interest')
```

```
    figure  
plot(lambda, diff_angle_1)  
axis([20 100 -90 90]);  
grid on;  
xlabel ('Wavelength (nm)')  
ylabel ('Diffraction angle for constant incident angle')
```

```
    figure  
plot(beta, lambda_1, beta, lambda_1/2, beta, lambda_1/3, beta,  
lambda_1/4, beta, lambda_1/5)  
axis([0 80 0 500]);  
grid on  
xlabel('diffraction angle');  
ylabel('wavelength nm');
```

```
    % grating mounting calculation  
lambda_1 = 25E-9;  
lambda_2 = 80E-9;  
beta_1 = asin((order*lambda_1/d) - sin(alpha_1));  
display(beta_1*180/pi);  
beta_2 = asin((order*lambda_2/d) - sin(alpha_1));
```

```

display(beta.2*180/pi);

% calculating b2
b2 = (cos(87 * pi/180) + cos(83 * pi/180) - (5.649 * (cos(83 * pi/180))^2)/0.2367 - (5.649 *
(cos(87 * pi/180))^2)/0.237)/(2 * (sin(83 * pi/180) + sin(83 * pi/180)));
display(b2);

% focus
r_1 = 0.237 * 5.649 * (cos(beta_1)^2)/(.237 * [cos(alpha_1) + cos(beta_1) - 2 * (sin(alpha_1) +
sin(beta_1)) * b2] - 5.649 * (cos(alpha_1)^2));
display(r_1);

r_2 = 0.237*5.649*(cos(beta_2)^2)/(.237*[cos(alpha_1) + cos(beta_2) - 2*(sin(alpha_1) +
sin(beta_2)) * b2] - 5.649 * (cos(alpha_1)^2));
display(r_2);

% resolution and dispersion
Disp = (d*cos(beta)*cos(phi))/Lb;
Disp = d.*cos((alphaRad)-(2*phi))/order; % at 1 meter
Res = N*d*(sin(alpha) + sin(beta))/lambda;

% Resolution in eV at 42 eV and Total spectral range for dispersion over 2 cm
Res = order*42.*cos(alphaRad)/(gr.den*spot);% If d is changed, change grooves/mm
Disp = ((42/50E-9)*d.*cos((alphaRad)-(2*phi))*2E-2/0.5)/order; % at 1 meter

Figure
plot(alpha,Res)
axis([0 90 0 .05]);
grid on
xlabel ('alpha in degrees')
ylabel ('Resolution (delta E) in eV at 42 eV')

figure
plot(alpha,Disp)
axis([0 90 0 30]);
grid on
xlabel('alpha in degrees')
ylabel('Linear Dispersion delta E over 2cm at 42eV')

```

A.2 Focal plane Curve Simulation

```
close all;
a = 85:0.1:88; %angle of incidence
l = 30:10:60; %wavelength range to be scanned in nm
d = 1E-3/1200; % groove spacing in meters
R = 5649; %Radius of curvature in mm
m = 1; % order
b2 = -20.119; % grating parameter
r = 237; %object distance

    for a = 85:1:88
for l = 30:10:60
disp('wavelength:')
disp(l)
disp('incident angle:')
disp(a)

$$b = a \sin d (12E - 4 * l - \sin d(a))$$


$$r1 = (r * R * (\cos d(b))^2) / (r * [\cos d(a) + \cos d(b) - 2 * b2 * (\sin d(a) + \sin d(b))] - R * (\cos d(a))^2)$$

t = 90 + b
z = r1*cosd(t)
x = r1*sind(t)
disp('—————')
end
end
```

Appendix B

FRED Simulation

FRED software is used to perform ray tracing for the curved VLS grating. Here are some basic tutorial of how to design optical setup in FRED.

B.1 Tutorial

Start by opening a new file in the software, in the left side there is tree of objects. First create a new subassembly by a right click on the geometry folder or by using *Ctrl + Atl + S*.

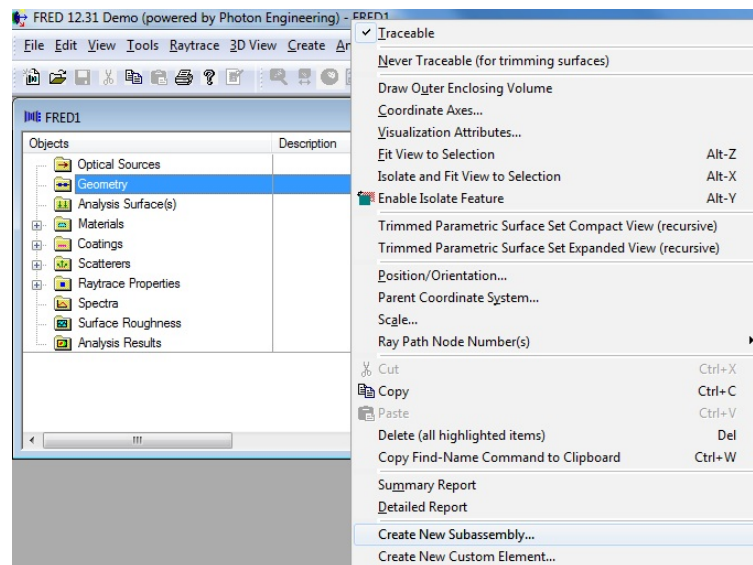


Figure B.1: Creating a new subassembly.

Next create an optical element, for example lens by right click on that new subassembly or by $Ctrl + Atl + L$.

Once lens is created, a new simplified optical source is created by right click on the optical

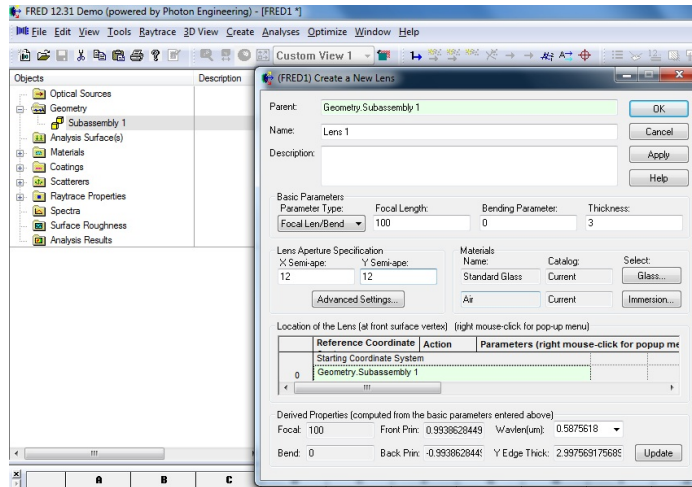


Figure B.2: Creating a new lens.

sources folder on the left side or by $Ctrl + Atl + I$. Select the optical source, in this case we have selected laser beam. Set all the parameters and the location of the source.

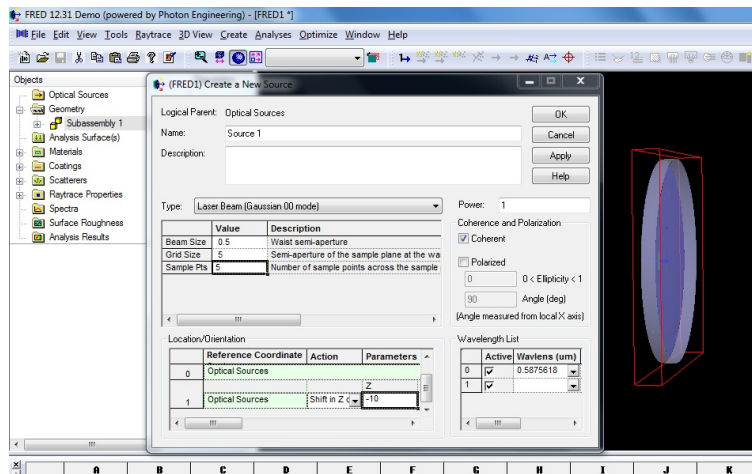


Figure B.3: Creating a new simplified source.

Now we create an analysis surface two study the image property at any place of interest. It can be created from left side tree or by using command $Ctrl + Alt + N$. Set the location of the analysis surface.

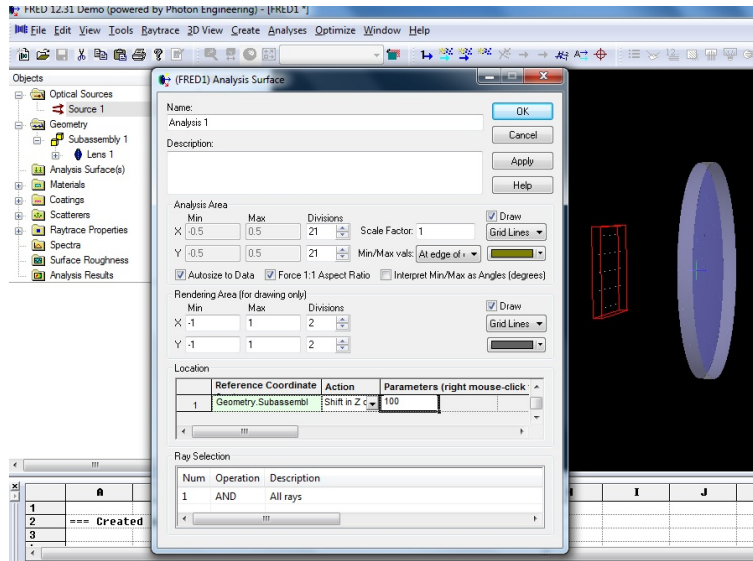


Figure B.4: Creating a new analysis surface.

Now give the command Trace and Render using *Ctrl + shift + F7*. After this any analysis could be performed using the created analysis surface.

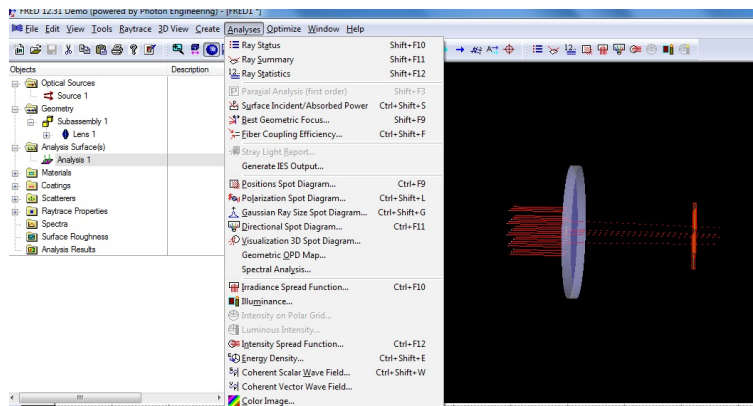


Figure B.5: Optical setup is complete now any analysis could be performed.

Bibliography

- [1] Ferray, M.; L’Huillier, A.; Li, X. F.; Lompre, L. A.; Mainfray, G.; Manus, C. *Journal of Physics B: Atomic, Molecular and Optical Physics* **1988**, *21*, L31.
- [2] Varj, K.; Johnsson, P.; Mauritsson, J.; LHuillier, A.; Lpez-Martens, R. *American Journal of Physics* **2009**, *77*.
- [3] Kapteyn, H. C.; Murnane, M. M.; Christov, I. P. *Physics Today* **2005**, *58*, 39.
- [4] Harada, T.; Sakuma, H.; Takahashi, K.; Watanabe, T.; Hara, H.; Kita, T. *Appl. Opt.* **1998**, *37*, 6803–6810.
- [5] McPherson, A.; Gibson, G.; Jara, H.; Johann, U.; Luk, T. S.; McIntyre, I. A.; Boyer, K.; Rhodes, C. K. *J. Opt. Soc. Am. B* **1987**, *4*, 595–601.
- [6] Lewenstein, M.; Balcou, P.; Ivanov, M. Y.; L’Huillier, A.; Corkum, P. B. *Phys. Rev. A* **1994**, *49*, 2117–2132.
- [7] *Optics Communications* **1971**, *2*, 391 – 395.
- [8] Schelev, M. Y.; Richardson, M. C.; Alcock, A. J. *Applied Physics Letters* **1971**, *18*.
- [9] Tsakiris, G. D.; Eidmann, K.; ter Vehn, J. M.; Krausz, F. *New Journal of Physics* **2006**, *8*, 19.
- [10] Nitzan, A.; Ratner, M. A. *Science* **2003**, *300*, 1384–1389.
- [11] Harada, T.; Kita, T. *Appl. Opt.* **1980**, *19*, 3987–3993.
- [12] Namioka, T. *J. Opt. Soc. Am.* **1959**, *49*, 446–460.
- [13] Harada, T.; Takahashi, K.; Sakuma, H.; Osyczka, A. *Appl. Opt.* **1999**, *38*, 2743–2748.
- [14] Kita, T.; Harada, T.; Nakano, N.; Kuroda, H. *Appl. Opt.* **1983**, *22*, 512–513.
- [15] Tokushima, T.; Harada, Y.; Watanabe, M.; Takata, Y.; Ishiguro, E.; Hiraya, A.; Shin, S. *Surface Review and Letters* **2002**, *09*, 503–508.
- [16] Wang, X.; Chini, M.; Cheng, Y.; Wu, Y.; Chang, Z. *Appl. Opt.* **2013**, *52*, 323–329.